

Impact of Temporal and Spatial Resolution on the Aeroacoustic Waves from a Two-dimensional Impinging Jet

T. Nonomura,* S. Tsutsumi,** R. Takaki,** E. Shima,** and K. Fujii*
Corresponding author: nonomura@flab.isas.jaxa.jp

* Institute of Space and Astronautical Science, Japan Aerospace Exploration Agency, Japan.

** JAXA's Engineering Digital Innovation Center, Japan Aerospace Exploration Agency, Japan.

Abstract: Impacts on the spatial and temporal resolutions are discussed through the two-dimensional model problem of jet impinging which is proposed by the present authors and Housman et al.[AIAA paper 2011-3650,2011]. The result shows that the high-resolution schemes improve the resolution of fine structures of vortices, though even a conventional scheme can predict the blast waves well. For solving the fine structure of vortices, high-order scheme is more than 10 times as efficient as conventional scheme.

Keywords: Numerical Algorithms, Computational Fluid Dynamics, Turbulence Modeling, Aeroacoustics.

1 Introduction

When rocket launches, there appear to be two severe acoustic loads on the pay-load. One is the ignition over pressure (IOP) which is a kind of blast wave generated when the rocket engine starts. The other is turbulent/shock noise generated by a rocket plume. It is important to predict both of them, accurately. Recently, the computational fluid dynamics starts to be used for the prediction of intensities of those acoustic waves.[1, 2, 3, 4, 5, 6] It is important to clarify the required spatial and temporal resolutions of the computational scheme/grid adopted in the simulation for the prediction of such an unsteady simulation. Thus far, the two-dimensional model problem of IOP is established by the present authors and Housman et al., and the series of analysis are conducted to understand the spatial and temporal resolution, as the part of collaboration work between NASA and JAXA which is now conducted.

Housman et al.[6]showed the criteria of number of the sub-iteration, tolerance of residual, and CFL for the accurate simulation, based on the database of the series of computation using three different grid resolution and conventional upwind scheme. It should be noted that they uses the Cartesian based computational grids and clearly discussed the grid resolution effects. Their analysis is very interesting and extension of their discussion to the high-resolution scheme, which is often used in the aero-acoustic and turbulent simulations, sounds very important.

Therefore, in this paper, we will present the effects of the spatial resolution of the computational schemes and grids on the resulting acoustic fields of the two-dimensional problem, whereas both of the conventional scheme and high-resolution scheme are examined. The difference in spatial resolution between conventional and high-order schemes is mainly discussed in this paper.

2 Problem Settings

A simplified two-dimensional jet impinging problem is proposed by the present authors and Housman et al. In this problem the simple geometry is introduced as shown in Fig. 1. There are modeled nozzle and inclined

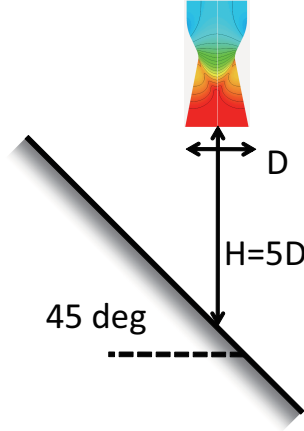


Figure 1: Geometry of the problem. Mach number contours are drawn in the nozzle.

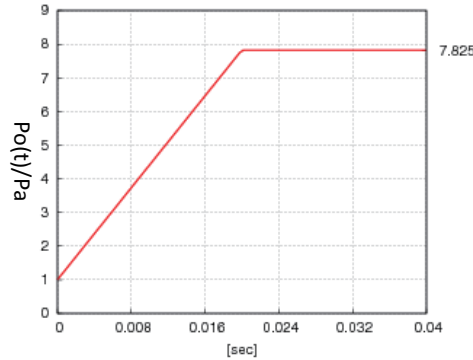


Figure 2: Pressure history of the chamber.

flat plate, which mimic the rocket launch site. The Mach 2 planner nozzle is assumed with straight wall at the nozzle skirt. For the nozzle inlet, the high pressure nozzle flow is imposed with time-depending chamber pressure history as shown in Fig. 2. At the final stage, the pressure ratio at between chamber and ambient conditions become 7.825. Moreover, the temperature ratio at between chamber and ambient conditions are set to be 1, that is corresponds to the cold jet assumption. The jet and ambient gas are assumed to be air and the specific heat ratio is set to 1.4. The flat plate has 45 [deg] angle, and distance from jet to plate (indicated as H in Fig. 1) is set to $5D$, where D is nozzle width.

With regard to the dimensionalization, we use following relations: ambient pressure $P_a = 0.1MPa$; ambient temperature $T_a = 300K$; sound speed of ambient condition $C_a = 347m/s$; nozzle exit diameter $D_e = 0.1m$; and time is set to D_e/C_a . With regard to the jet inflow condition, Mach number is extrapolated from the one-point inside the boundary and quasi-one-dimensional relationship is adopted with the isentropic assumption. Pressure histories at the nozzle inlet and exit are shown in the Fig. 3. These profiles do not change for any computational grids and codes as discussed later. Finally, locations of the numerical probes are shown in Fig. 4. The data obtained at these points are discussed.

3 Computational Grids and Codes

Two types of computational grids are adopted in this study. One is fully curvilinear grids manufactured by the present authors, and the other is Cartesian/curvilinear combined grids created by Housman et al. The former grids are shown in Fig. 5. For this grid, two computational codes in JAXA are adopted for solving the proposed problem; one is UPACS[7, 8] (which is called as Code 1) which is finite volume structured code, and the other is LANS3D (which is called as Code 2)[9] which is finite difference structured code. Code 1

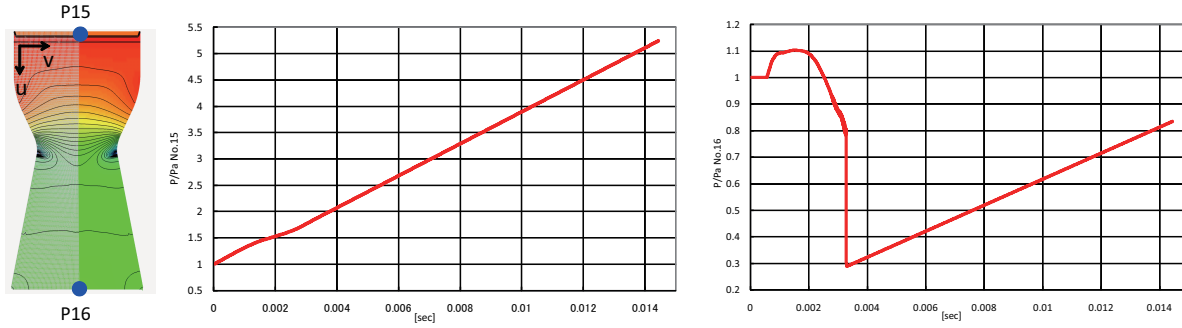


Figure 3: Pressure histories at the nozzle inlet and exit.

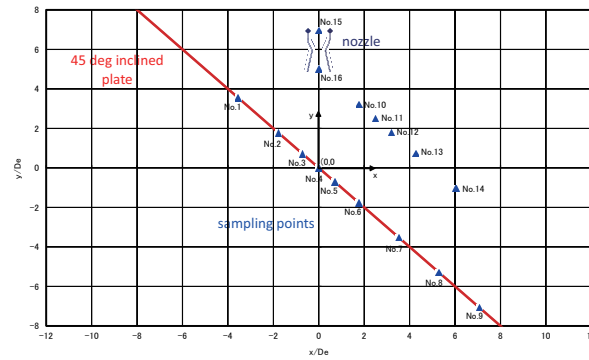


Figure 4: Locations of numerical probes.

(UPACS) is used for survey of effective time step and number of subiterations as discussed in the Section 4.2. Both code 1 (UPACS) and 2 (LANS3D) are used for the survey of spatial resolution when using high order schemes.

On the other hand, latter grids used as shown in Fig. 6 in the study by Housman et al. are also used for the comparison of different codes in NASA and JAXA, as the collaboration works between NASA and JAXA. For this, results of Code 2 and the computational code adopted by NASA (LAVA)[6] are compared using the latter grids.

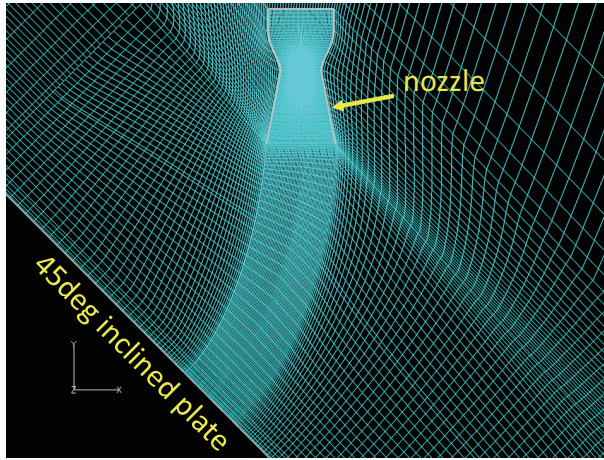


Figure 5: Fully curvilinear grids created by the present authors group.

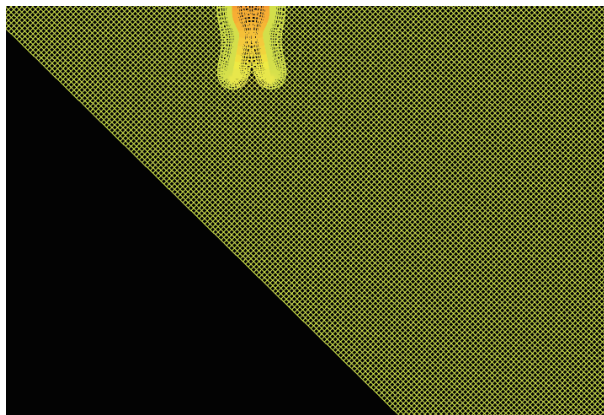


Figure 6: Cartesian/curvilinear grids created by the Housman et al.[6]

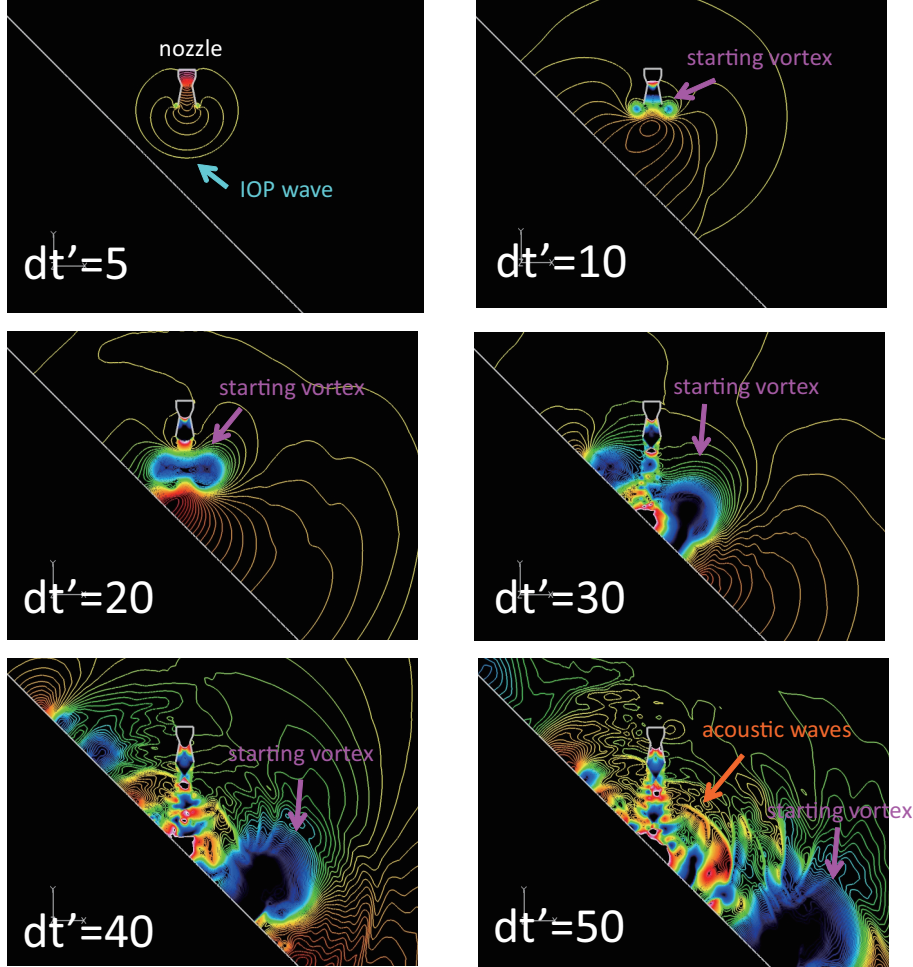


Figure 7: Pressure history of the chamber.

4 Results and Discussions

4.1 Representative Results of The Problem

The visualization of representative results of the problem discussed here is shown in Fig. 7. First, the starting vortex is generated at the nozzle lip, and they impinge to the plate with generating the acoustic waves. The time history of the corresponding data at the numerical probe No. 10 is shown in Fig. 8. There are characteristic profiles in the pressure time history: 1) high pressure region by ignition overpressure (IOP) 2) low pressure region by starting vortex, and 3) high frequency fluctuations due to shear layer.

4.2 Efficient Time Step and Numbers of Subiterations

The fully curvilinear grids and the Code 1 (UPACS) in JAXA are used, and the efficient time step and numbers of subiterations are discussed. The conventional numerical methods are used: second-order monotonically upwind scheme for conservation law (MUSCL)[10] with Roe's flux difference splitting (FDS)[11] is adopted for the spatial differencing; the matrix-free Gauss-Seidel (MFGS) or total variation diminishing Runge-Kutta[12] is used for time integration.

Table 1 presents the cases examined in this study. The pressure histories at numerical probe No 10 for cases with CFL numbers 10 and 1 are shown in Figs. 9 and 10, here CFL number for the fully curvilinear grids is defined as approximated maximum CFL number. With increasing the number of subiterations for the case with CFL number 10, the solution is converged to the solution of explicit time integration, while the

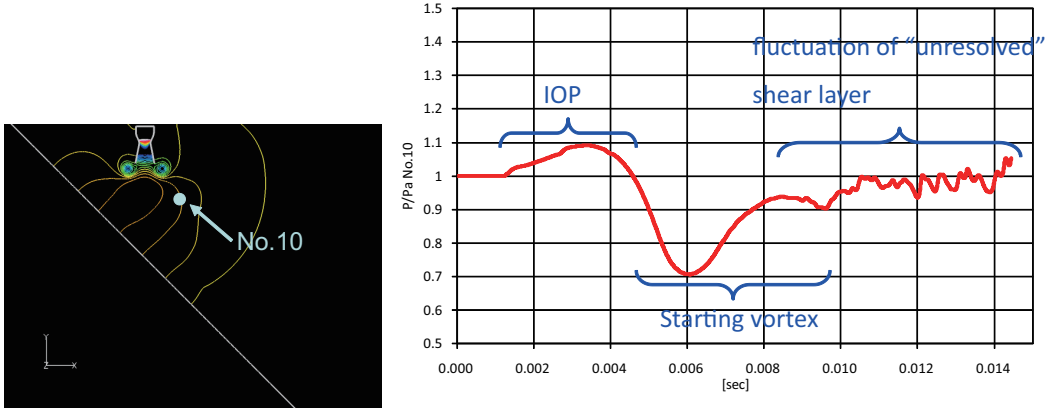


Figure 8: Pressure history of the chamber.

number of subiteration does not affect the solution of the cases with CFL number 1. If the convergence is not achieved, propagation speed of the IOP wave decreases, and the intensity of the starting vortex increases. In this study, we judge the convergence of the solution whether the difference between first minimum pressure value and that for the reference solution is less than 0.05. The convergence status for each case is shown in Table ???. Among the cases, the most efficient solution are obtained by comparing the computational times. With Code 1 (UPACS) and fully curvilinear grids, the combinations of CFL number of 5 and subiteration of 5 times, or CFL number of 2 and subiteration of 2 are efficient. This is similar results by Housman et al. and we have optimal CFL number and number of subiterations: optimal CFL number is order of $O(1)$.

Table 1: Computational cases for investigating efficient time step and number of subiterations.

case	CFL	$dt[\mu\text{ sec}]$	subiterations
1	10	8.6	2
2	10	8.6	3
3	10	8.6	5
4	10	8.6	10
5	5	4.3	2
6	5	4.3	3
7	5	4.3	5
8	5	4.3	10
9	2	1.7	2
10	2	1.7	3
11	2	1.7	5
12	2	1.7	10
13	1	0.86	2
14	1	0.86	3
15	1	0.86	5
16	1	0.86	10
17	0.5	0.43	2
18	0.5	0.43	3
19	0.5	0.43	5
20	0.5	0.43	10
21	1	0.86	TVD-RK(3)

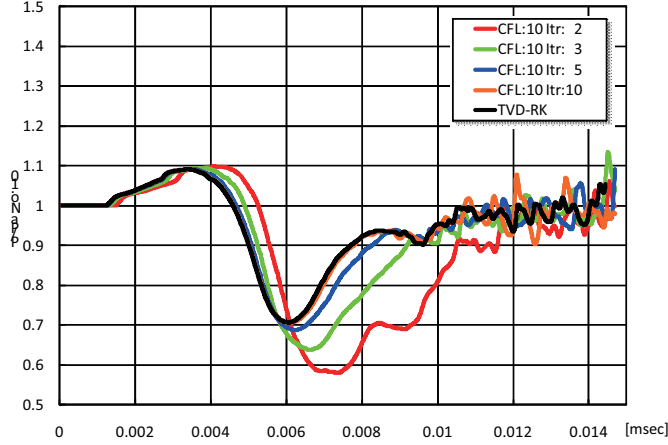


Figure 9: Pressure history at No. 10 under CFL condition of 10 with Code 1.

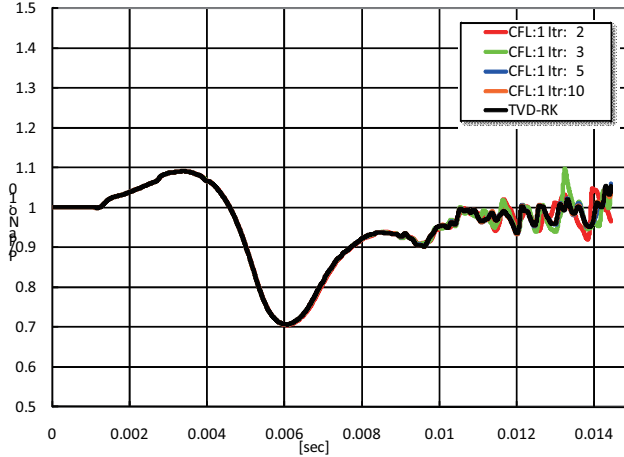


Figure 10: Pressure history at No. 10 under CFL condition of 1 with Code 1.

4.3 Impacts of High-order Schemes

The impacts of the high-order schemes are discussed here, using fully curvilinear grids. Both Code 1 (UPACS) and Code 2 (LANS3D) have conventional-scheme and high-order-scheme options. The results of Code 2 (LANS3D) with the conventional scheme are almost the same as that of Code 1 (UPACS) with the conventional scheme, and they are omitted for brevity. With regard to the Code 1 (UPACS) with the conventional scheme, second-order MUSCL scheme with Roe's FDS is adopted for the spatial differencing. For the Code 1 (UPACS) with the high-order scheme, compact scheme[13, 14, 15] with localized artificial diffusivity[16, 17] is adopted for spatial differencing. Meanwhile, for the Code 2 (LANS3D) with the high-order scheme, seventh order modified weighted compact nonlinear scheme (WCNS)[18, 19, 20, 21] is adopted. For all the cases, TVD-RK is used for the time integration.

The snapshots of the flow fields (density fields) are shown in Fig. 11 and the pressure histories at the numerical probe No. 10 are shown in Fig. 12. Figure 11 shows that the shear layer behaviors are quite different when using high-order schemes. Especially, fine-scale vortices are resolved for the high-order schemes, and the notable dip appears at $t = 0.0065[\text{sec}]$ as shown in Fig. 12 for the case of Code 2 with WCNS, though the pressure profiles at $t < 0.006[\text{sec}]$, which represents the pressure waves, are almost the same. Among the three results, fluctuations at $t < 0.01$ are the strongest for the Code 2 with WCNS, and this illustrates that WCNS has the highest resolution in this study. As discussed by the present authors,

Table 2: Wall clock time and convergence status for each case.

case	CFL	$dt[\mu\text{sec}]$	subiterations	wall clock time[sec]	convergence
1	10	8.6	2	378	Not converged
2	10	8.6	3	374	Not converged
3	10	8.6	5	872	Not converged
4	10	8.6	10	1483	Converged
5	5	4.3	2	603	Not converged
6	5	4.3	3	754	Not converged
7	5	4.3	5	1209	Converged
8	5	4.3	10	2387	Converged
9	2	1.7	2	1227	Converged
10	2	1.7	3	1579	Converged
11	2	1.7	5	2499	Converged
12	2	1.7	10	4901	Converged
13	1	0.86	2	2060	Converged
14	1	0.86	3	2996	Converged
15	1	0.86	5	4948	Converged
16	1	0.86	10	9763	Converged
17	0.5	0.43	2	4083	Converged
18	0.5	0.43	3	6202	Converged
19	0.5	0.43	5	9988	Converged
20	0.5	0.43	10	19751	Converged
21	1	0.86	TVD-RK(3)	2370	Reference solution

the efficiency of WCNS for two-dimensional problem is almost 10 times higher than conventional scheme. It should be noted that, however, the WCNS is less robust, and WCNS with CFL number of 5 and implicit scheme blow up during the computation.

4.4 Code-to-code Comparison

Finally, the code-to-code comparison between NASA and JAXA is conducted. For the computational grid, Cartesian/curvilinear grids provided by NASA are used. There are three grids with different resolution: fine (1,945,000 grid points), medium (552,000 grid points), and coarse (165k grid points). For the comparison, Code 2 (LANS3D) and the computational code by NASA (LAVA) are used. With regard to the Code 2 (LANS3D) with the conventional scheme, second-order MUSCL and simple high-resolution upwind scheme (SHUS)[22] are used for spatial differencing, and ADI-SGS scheme[23] is used for time integration. For the Code 2 (LANS3D) with the high-order scheme, seventh order modified weighted compact nonlinear scheme (WCNS) is adopted, while ADI-SGS scheme is used for time integration as similar to the conventional option. Meanwhile, for LAVA (NASA code), second-order MUSCL and Roe’s FDS and line implicit time integration is used. Here, time steps for Code 1 are set to $0.57 \mu\text{sec}$ which is small enough, and time steps for LAVA (NASA code) are set to the optimum value as investigated by Housman et al.

The snapshots of the flow fields (density fields) are shown in Fig. 13 and the pressure histories at the numerical probe No. 10 for each case are shown in Figs. 14, 15, and 16. The pressure time histories of the Code 2 (LANS3D) with conventional scheme and LAVA (NASA code) are almost identical for each grid resolution (coarse, medium, and fine), while the resolution of Code 2 (LANS3D) is slightly higher than LAVA (NASA code). On the other hand, that for the Code 2 (LANS3D) with high-order scheme (WCNS) has significantly high resolution compared with the conventional scheme. Especially, for the shear layer fluctuation part ($t > 0.10$), very fine structures are well captured for high-order scheme. Comparing Code 2 (LANS3D) with WCNS on the coarse grid and conventional schemes on the fine grid, almost the same resolutions are obtained for shear layer fluctuation, while the resolution for initial pressure wave does not change much. This implies that the computational costs of WCNS are almost 16 times less than conventional

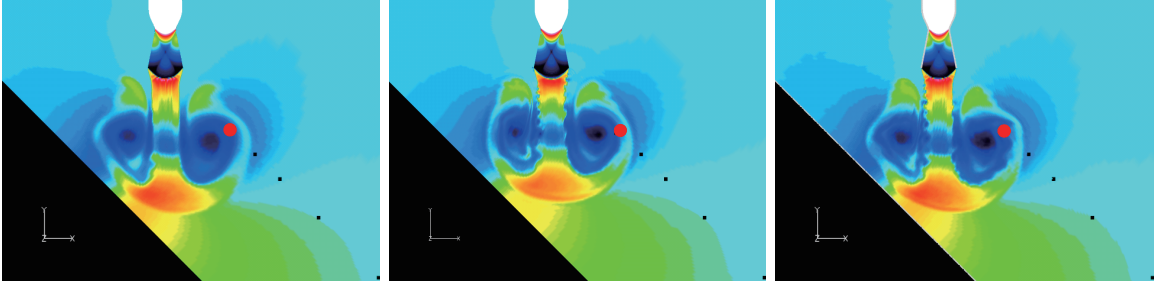


Figure 11: Instantaneous flow fields. From left to right, Code 1 MUSCL, Code 1 compact scheme and LAD, and Code 2 WCNS.

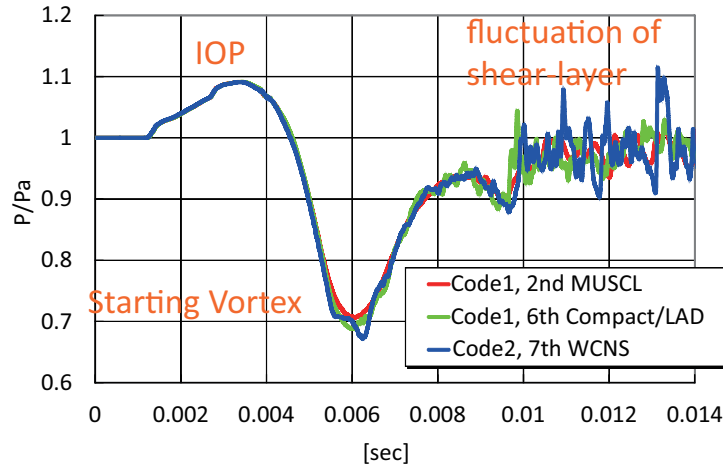


Figure 12: Pressure history at No. 10 for Code 1 MUSCL, Code 1 compact scheme and LAD, and Code 2 WCNS.

scheme if the target is shear layer fluctuation, whereas the spatial resolutions in a two-dimensional problem is only considered. Besides, the time integration for WCNS is severer as discussed in the previous subsection.

5 Conclusion and Future Work

Impacts on the spatial and temporal resolutions are discussed through the two-dimensional model problem of jet impinging which is proposed by Housman et al. and the present authors. The result shows that the high-resolution schemes improve the resolution of fine structure of vortices, though a conventional scheme can predict the blast waves well. For solving the fine structure of vortices, high-order scheme is more than 10 times as efficient as conventional scheme.

References

- [1] Kozo Fujii, Taku Nonomura, and Seiji Tsutsumi. Toward accurate simulation and analysis of strong acoustic wave phenomena - a review from the experience of our study on rocket problems. *International Journal for Numerical Methods in Fluids*, 64(10-12):1412–1432, 2010.
- [2] Taku Nonomura, Yoshinori Goto, and Kozo Fujii. Acoustic waves from a supersonic jet impinging on an inclined flat plate. In *AIAA-2010-476*, 2010.
- [3] Taku Nonomura, Yoshinori Goto, and Kozo Fujii. Aeroacoustic waves generated from a supersonic jet impinging on an inclined flat plate. *International Journal of Aeroacoustics*, 10(4):401–426, 2011.

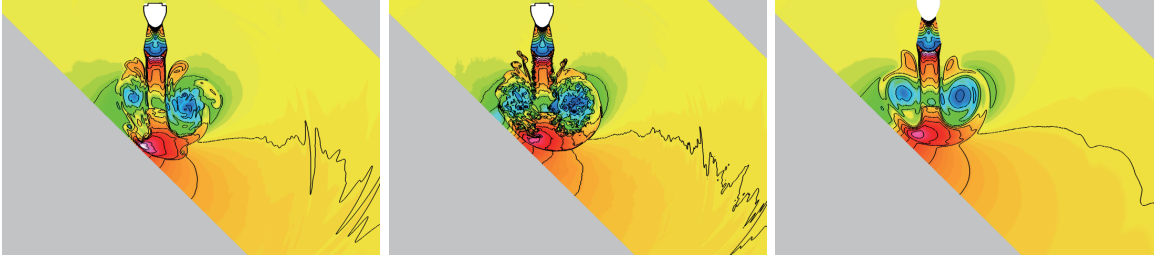


Figure 13: Instantaneous flow fields using Cartesian/curvilinear grids. From left to right, Code 2 MUSCL, Code 2 WCNS, and LAVA MUSCL(NASA).

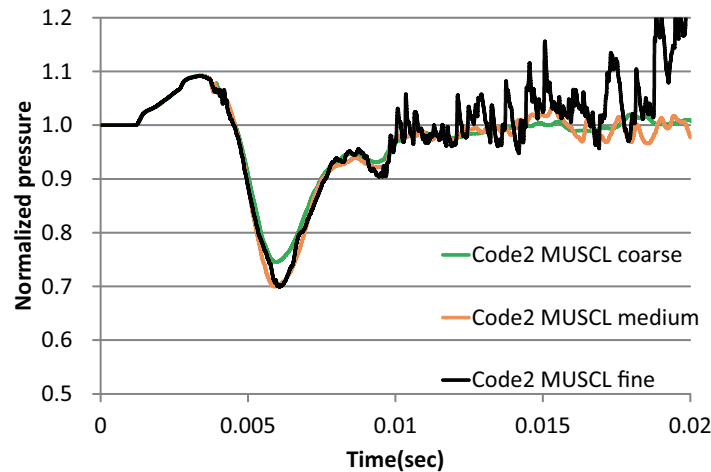


Figure 14: Pressure history of No. 10 with Cartesian grids using Code 2 MUSCL.

- [4] Seiji Tsutsumi, Susumu Kato, Kota Fukuda, Ryoji Takaki, and Kyoichi Ui. Effect of deflector shape on acoustic field of launch vehicle at lift-off. In *AIAA-2009-328*, 2009.
- [5] Seiji Tsutsumi, Ryoji Takaki, Yuta Nakanishi, Koji Okamoto, and Susumu Teramoto. Numerical study on acoustic radiation from a supersonic jet impinging to an inclined plate. In *AIAA 2011-2922*, 2011.
- [6] Jeffrey A. Housman, Michael F. Barad, and Cetin C. Kiris. Space-time accuracy assessment of cfd simulations for the launch environment. In *AIAA Paper 2011-3650*, 2011.
- [7] Takashi Yamane, Kazuomi Yamamoto, Shunji Enomoto, Hiroyuki Yamazaki, Ryoji Takaki, and Toshiyuki Iwamiya. Development of a common cfd platform-upacs. In *Parallel Computational Fluid Dynamics-Proceedings of the Parallel CFD 2000 Conference, Trondheim, Norway, Elsevier Science BV*, pages 257–264, 2001.
- [8] Taro Imamura, Shunji Enomoto, Yuzuru Yokokawa, and Kazuomi Yamamoto. Three-dimensional unsteady flow computations around a conventional slat of high-lift devices. *AIAA Journal*, 46(5):1045–1053, 2008.
- [9] Kozo Fujii and Shigeru Obayashi. High-resolution upwind scheme for vortical-flow simulations. *Journal of Aircraft*, 26(12):1123–1129, December 1989.
- [10] Bram van Leer. Towards the ultimate conservation difference scheme. v. a second-order sequel to godunov’s method. *Journal of Computational Physics*, 32:101–136, 1979.
- [11] Philip L. Roe. Approximate riemann solvers, parameter vectors, and difference scheme. *Journal of Computational Physics*, 43(2):357–372, 1981.
- [12] Sigal Gottlieb and Chi-Wang Shu. Total variation diminishing runge-kutta schemes. *Mathematics of Computation*, 67(221):73–85, 1998.

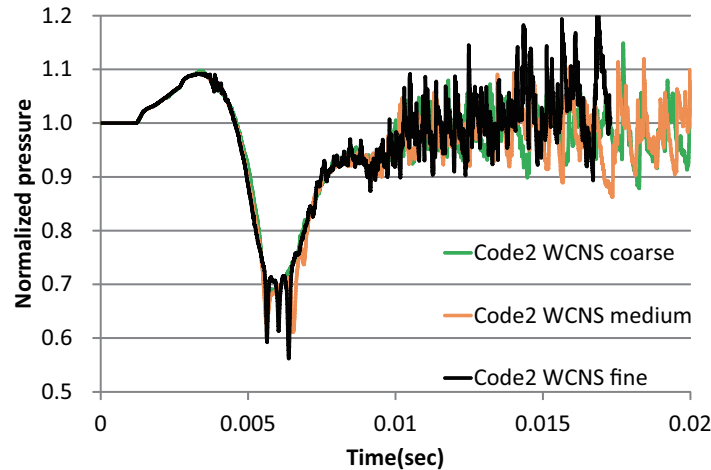


Figure 15: Pressure history of No. 10 with Cartesian grids using Code 2 WCNS.

- [13] Sanjiva K. Lele. Compact finite difference schemes with spectral-like resolution. *Journal of Computational Physics*, 103(1):16–42, 1992.
- [14] Datta V. Gaitonde and Miguel R. Visbal. Padé-type higher-order boundary filters for the navier-stokes equations. *AIAA Journal*, 38(11):2103–2112, 2000.
- [15] Marcelo H. Kobayashi. On a class of pade finite volume methods. *Journal of Computational Physics*, 156:137–180, 1999.
- [16] Andrew W. Cook and William H. Cabot. Hyperviscosity for shock-turbulence interactions. *Journal of Computational Physics*, 203:379–385, 2005.
- [17] Soshi Kawai and Kozo Fujii. Compact scheme with filtering for large-eddy simulation of transitional boundary layer. *AIAA Journal*, 46(3):690–700, March 2008.
- [18] Taku Nonomura, Nobuyuki. Iizuka, and Kozo. Fujii. Increasing order of accuracy of weighted compact nonlinear scheme. In *AIAA-2007-893*, 2007.
- [19] Taku Nonomura and Kozo Fujii. Effects of difference scheme type in high-order weighted compact nonlinear schemes. *Journal of Computational Physics*, 228:3533–3539, 2009.
- [20] Taku Nonomura, Nobuyuki Iizuka, and Kozo Fujii. Freestream and vortex preservation properties of high-order weno and wcns on curvilinear grids. *Computers & Fluids*, 39(2):197–214, 2010.
- [21] Taku Nonomura, Weipeng Li, Yoshinori Goto, and Kozo Fujii. Efficiency improvements in seventh-order weighted compact nonlinear scheme. *CFD Journal*, 18(2):180–186, 2011.
- [22] Eiji Shima and Tadamasa Jounouchi. Role of CFD in aeronautical engineering (No.14) - AUSM type upwind schemes-. In *Proceedings of the 14th NAL Symposium on Aircraft Computational Aerodynamics*, pages 7–12. NAL, 1997.
- [23] Hiroyuki Nishida and Taku Nonomura. Adi-sgs scheme on ideal magnetohydrodynamics. *Journal of Computational Physics*, 228:3182–3188, 2009.

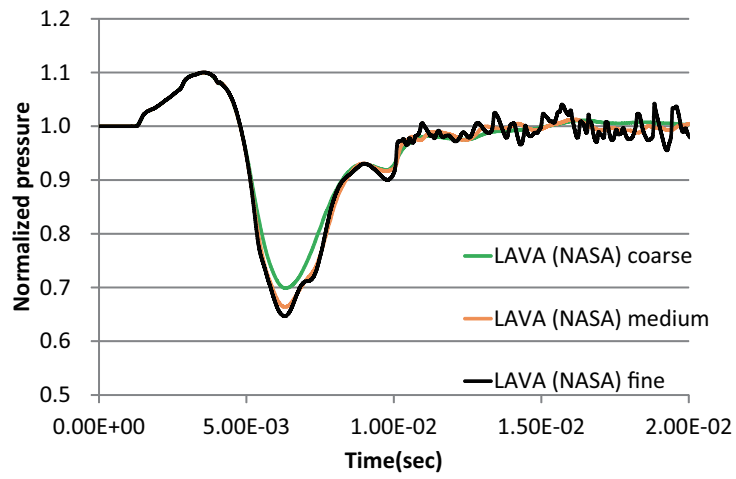


Figure 16: Pressure history of No. 10 with Cartesian grids using LAVA.